



Model for the dynamics of a bubble undergoing small shape oscillations between elastic layers

Yurii A. Ilinskii, Todd A. Hay, Evgenia A. Zabolotskaya, and Mark F. Hamilton

Citation: [AIP Conference Proceedings](#) **1474**, 147 (2012); doi: 10.1063/1.4749317

View online: <http://dx.doi.org/10.1063/1.4749317>

View Table of Contents: <http://scitation.aip.org/content/aip/proceeding/aipcp/1474?ver=pdfcov>

Published by the [AIP Publishing](#)

Articles you may be interested in

[Integral wall model for large eddy simulations of wall-bounded turbulent flows](#)

Phys. Fluids **27**, 025112 (2015); 10.1063/1.4908072

[Transition between regimes of a vertical channel bubbly upflow due to bubble deformability](#)

Phys. Fluids **25**, 102110 (2013); 10.1063/1.4824006

[Model for the dynamics of a spherical bubble undergoing small shape oscillations between parallel soft elastic layers](#)

J. Acoust. Soc. Am. **134**, 1454 (2013); 10.1121/1.4812864

[Numerical simulation of multiple bubbles growing in a Newtonian liquid filament undergoing stretching](#)

Phys. Fluids **18**, 042106 (2006); 10.1063/1.2194931

[The steady propagation of a bubble in a flexible-walled channel: Asymptotic and computational models](#)

Phys. Fluids **14**, 443 (2002); 10.1063/1.1432694

Model for the Dynamics of a Bubble Undergoing Small Shape Oscillations between Elastic Layers

Yurii A. Ilinskii, Todd A. Hay,
Evgenia A. Zabolotskaya and Mark F. Hamilton

Applied Research Laboratories, The University of Texas at Austin, Austin, Texas 78713–8029

Abstract. A model is presented for a pulsating and translating gas bubble in a channel formed by two soft elastic parallel layers. The bubble is free to undergo small shape deformations. Coupled nonlinear second-order differential equations are obtained for the shape and position of the bubble, and numerical integration of an expression for the liquid velocity at the layer interfaces yields an estimate of their displacement. Simulations reveal behavior consistent with laboratory observations.

Keywords: bubble dynamics, tissue interaction

PACS: 43.35.Ei

INTRODUCTION

Photographs of acoustically-excited ultrasound contrast agent microbubbles in *ex vivo* blood vessels have revealed that the bubbles translate and form jets toward the center of the vessel and that the associated vessel displacement is often asymmetric. [1, 2] These observations have motivated the development of a model for aspherical bubble dynamics between elastic layers and in blood vessels.

THEORY

The geometry is illustrated in Fig. 1. Two incompressible elastic layers with density ρ , thicknesses h_1 and h_2 , shear moduli μ_1 and μ_2 , and with their surfaces perpendicular to the z axis, are immersed in an incompressible liquid also with density ρ . A bubble is positioned between the two layers. The surface of the bubble relative to its local spherical coordinate system centered at location $Z(t)$ along the z axis may be written [3, 4]

$$\mathbf{r}_s(t, \theta) = \left[R(t)P_0(\cos \theta) + \sum_{n=2}^{\infty} s_n(t)P_n(\cos \theta) \right] \mathbf{e}_r, \quad (1)$$

where t is time, \mathbf{e}_r is a unit vector pointing outward from the center of the bubble, P_n are Legendre polynomials, and $s_n(t)$ are time-dependent expansion coefficients. It is assumed that the surface mode amplitudes are small compared to the radius, i.e., $|s_n| \ll R$ for $n \geq 2$. For simplicity, in the present work the summation in Eq. (1) is truncated at $n=3$ (octupole mode), the lowest-order mode capable of capturing jet initiation.

The kinetic and potential energies of the system are now presented, followed by coupled nonlinear dynamical equations for the bubble shape and the motion of the layers.

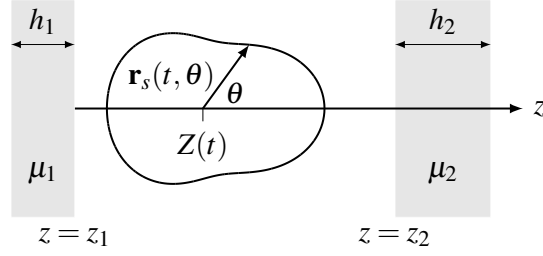


FIGURE 1. Geometry and coordinate system for a spherical bubble with shape perturbations at location $z = Z(t)$ between two elastic layers.

Kinetic energy

Since the layers are assumed to be incompressible with density equal to that of the liquid, the kinetic energy is calculated by considering the motion of an unbounded liquid surrounding the bubble. Letting $U = \dot{Z}$ designate the translational velocity of the bubble, we obtain for the kinetic energy

$$\begin{aligned} \mathcal{K} = 2\pi R^2 & \left[R\dot{R}^2 + \frac{1}{6}RU^2 + R \left(\frac{s_2^2}{15} + \frac{s_3^2}{28} \right) - \frac{U^2}{10}s_2 + \dot{R} \left(\frac{2}{3}s_2\dot{s}_2 + \frac{3}{7}s_3\dot{s}_3 \right) \right. \\ & \left. - \frac{U}{35} \left(2s_3\dot{s}_2 + \frac{3}{2}s_2\dot{s}_3 \right) + \frac{s_2^2}{5R} \left(\frac{1}{3}\dot{R}^2 + \frac{27}{35}U^2 \right) + \frac{s_3U}{35R} \left(11s_2\dot{R} + \frac{9}{7}s_3U \right) \right]. \quad (2) \end{aligned}$$

Potential energy

Potential energy stored via surface tension, gas compression, and displacement of the elastic layers is included. Expressions for the potential energy associated with gas compression and surface tension are

$$\mathcal{V}_g = \frac{4}{3}\pi R_e^3 \left(P_0 + \frac{P_l}{\gamma - 1} \right), \quad \mathcal{V}_\sigma = 4\pi\sigma \left(R_e^2 + \frac{2}{5}s_2^2 + \frac{5}{7}s_3^2 \right),$$

respectively, where $R_e = (3V/4\pi)^{1/3}$ is the effective radius of the bubble, V the bubble volume, P_l the pressure in the liquid at the bubble wall (including any applied acoustic pressures), γ the polytropic exponent, and σ surface tension. The strain energy density in the j^{th} elastic layer due to shear deformation may be expressed in terms of the strain tensor components E_{ii} as $\mu_j(E_{rr}^2 + E_{\theta\theta}^2 + E_{\phi\phi}^2)$. Integration over the volume of the layer yields

$$\mathcal{V}_j = \frac{\pi\mu_j h_j}{3} \left[\frac{R_e^6}{(Z - z_j)^4} - \frac{8R_e^3 R_0^3}{(Z_0 - z_j)(Z - z_j)(Z + Z_0 + 2z_j)^2} + \frac{R_0^6}{(Z_0 - z_j)^4} \right] \quad (3)$$

for the energy, where $Z_0 = Z(0)$. The total potential energy is $\mathcal{V} = \mathcal{V}_g + \mathcal{V}_\sigma + \mathcal{V}_1 + \mathcal{V}_2$.

Dynamical equations for the bubble and elastic layers

The dynamical equations are obtained by substituting the kinetic and potential energies into Lagrange's equation. The equation for the effective radius R_e is

$$\begin{aligned}
 R_e \ddot{R}_e + \frac{3}{2} \dot{R}_e^2 = & \frac{P_l}{\rho} + \frac{1}{4} U^2 + \frac{1}{2} \left(\frac{s_2^2}{3} + \frac{s_3^2}{4} \right) + \frac{s_2 \dot{s}_2}{15} + \frac{s_3 \dot{s}_3}{14} + \frac{\dot{R}_e}{R_e} \left(\frac{2}{15} s_2^2 + \frac{1}{7} s_3^2 \right) \\
 & + \frac{\dot{R}_e^2}{R_e^2} \left(\frac{s_2^2}{15} + \frac{s_3^2}{14} \right) + \frac{2\dot{R}_e}{R_e} \left(\frac{2}{15} s_2 \dot{s}_2 + \frac{s_3 \dot{s}_3}{7} \right) - \frac{11}{70} \frac{s_2 s_3}{R_e} \dot{U} \\
 & - \frac{U}{R_e} \left(\frac{1}{5} s_2 \dot{s}_3 + \frac{3}{14} \dot{s}_2 s_3 \right) - \frac{U^2}{10 R_e} \left(s_2 + \frac{17}{98} \frac{s_3^2}{R_e} - \frac{19}{70} \frac{s_2^2}{R_e} \right) \\
 & - \sum_{j=1}^2 \frac{\beta_j}{2} \left[\frac{R_e^3}{(Z-z_j)^4} - \frac{4R_0^3}{(Z_0-z_j)(Z-z_j)(Z_0+Z-2z_j)^2} \right], \quad (4)
 \end{aligned}$$

where $\beta_j = \mu_j h_j / \rho$. The corresponding equation for the bubble position $Z = \int U dt$ is

$$\begin{aligned}
 \frac{R_e^3}{3} \dot{U} + R_e^2 \dot{R}_e U = & \frac{R_e^2}{5} \left(s_2 \dot{U} + \dot{s}_2 U + \frac{3}{14} s_2 \dot{s}_3 + \frac{2}{7} s_3 \dot{s}_2 + \frac{1}{2} \dot{s}_2 \dot{s}_3 \right) - \frac{\dot{U} R_e}{35} \left(\frac{19}{5} s_2^2 + \frac{17}{7} s_3^2 \right) \\
 & + \frac{2UR_e}{5} \left(s_2 \dot{R}_e + \frac{17}{49} s_3 \dot{s}_3 - \frac{19}{35} s_2 \dot{s}_2 \right) - \frac{\dot{R}_e U}{35} \left(\frac{19}{5} s_2^2 - \frac{17}{7} s_3^2 \right) \\
 & - \frac{11}{35} s_2 s_3 R_e \left(\ddot{R}_e + \frac{\dot{R}_e^2}{R_e} \right) - \frac{\dot{R}_e R_e}{5} \left(\frac{8}{7} s_2 \dot{s}_3 + \dot{s}_2 s_3 \right) \\
 & + \frac{2R_e^3}{3} \sum_{j=1}^2 \frac{\beta_j}{(Z-z_j)^2} \left[\frac{R_e^3}{(Z-z_j)^3} - \frac{2R_0^3 (Z_0+3Z-4z_j)}{(Z_0-z_1)(Z_0+Z-2z_j)^3} \right]. \quad (5)
 \end{aligned}$$

Similar second-order differential equations are obtained for the quadrupole and octupole mode amplitudes s_2 and s_3 , which must be omitted here due to space restrictions.

The i^{th} component of the velocity vector for a point at the interface of the j^{th} elastic layer is

$$\dot{x}_i = \frac{R_e^2 \dot{R}_e}{r_j^3} [x_i - (Z-z_j) \delta_{iz}] - \frac{R_e^3 U}{2r_j^3} \left\{ \delta_{iz} - \frac{3}{r^2} [x_i - (Z-z_j) \delta_{iz}] [z - (Z-z_j)] \right\}, \quad (6)$$

where r_j is the distance from the bubble location Z to the point on the interface. Equation (6) may be integrated numerically to obtain an estimate of the layer displacement.

SIMULATION EXAMPLE

Parameters selected for the simulation correspond to a gas bubble with equilibrium radius of $R_0 = 1.5 \mu\text{m}$ oscillating in a blood vessel of width $z_2 - z_1 = 5R_0$. The viscosity and surface tension of the blood are $\eta = 5 \text{ mPa}\cdot\text{s}$ and $\sigma = 0.06 \text{ N/m}$, respectively, and the vessel walls (elastic layers) have $\beta_1 = \beta_2 = 0.01 \text{ m}^3/\text{s}^2$. [5] The system is initially

at rest and at equilibrium with the bubble center positioned a distance $Z_0 - z_1 = 1.5R_0$ from the left elastic layer in Fig. 1.

Figure 2(a) shows the time evolution of the amplitudes of the bubble radius and quadrupole and octupole modes when the system is driven by 5 cycles of a sinusoidal acoustic pressure with amplitude 330 kPa and frequency 2.9 MHz (the natural frequency of the bubble). The position of the bubble is shown in Fig. 2(b). Snapshots of the system at times $t = 0, 0.45$ and $0.79 \mu\text{s}$ are shown in Fig. 3, corresponding to the initial state (a), and first (b) and second (c) collapses. As Fig. 2 shows, peaks in the amplitudes of the

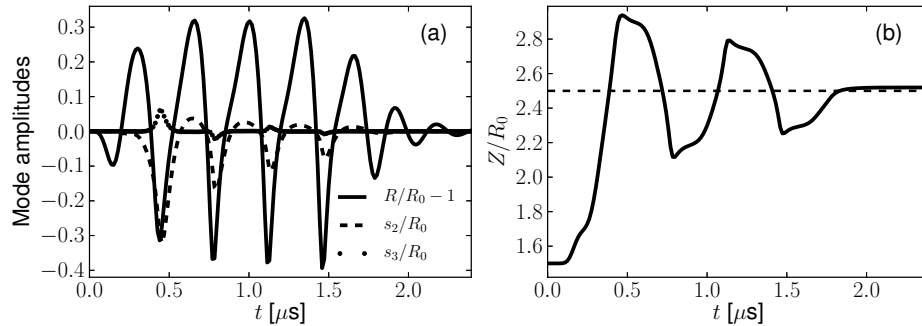


FIGURE 2. (a) Bubble mode amplitudes, (b) bubble position.

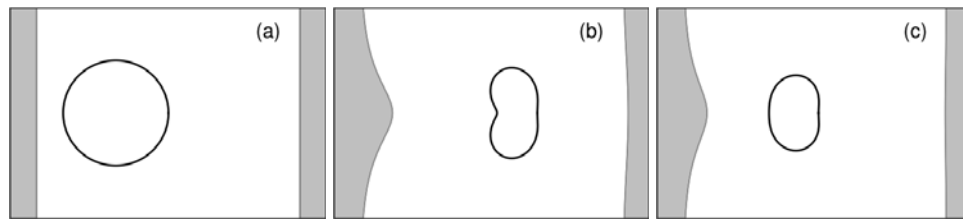


FIGURE 3. Snapshots at (a) $t = 0$, (b) $t = 0.45$, and (c) $t = 0.79 \mu\text{s}$.

surface modes s_2 and s_3 , indicating the formation of a jet [see Fig. 3(b)], tend to occur at instants of high translational velocity. Examination of Fig. 2(b) also shows that the bubble tends to translate towards the center of the channel (dashed line at $Z/R_0 = 2.5$). Note also in Fig. 3 that the vessel walls tend to move inward, thereby decreasing the channel width. These trends are consistent with laboratory measurements. [1, 2]

ACKNOWLEDGMENTS

This work was supported by NIH grant numbers DK070618 and EB011603.

REFERENCES

1. H. Chen, W. Kreider, A. A. Brayman, M. R. Bailey, and T. J. Matula, *Phys. Rev. Lett.* **106**, 034301 (2011).
2. H. Chen, A. A. Brayman, W. Kreider, M. R. Bailey, and T. J. Matula, *Ultrasound Med. Biol.* **37**, 2139–2148 (2011).
3. A. A. Doinikov, *J. Fluid Mech.* **501**, 1–24 (2004).
4. E. Kurihara, T. A. Hay, Yu. A. Ilinskii, E. A. Zabolotskaya, and M. F. Hamilton, *J. Acoust. Soc. Am.* **130**, 3357–3369 (2011).
5. J. B. Freund, *J. Acoust. Soc. Am.* **123**, 2867–2874 (2008).